

## **Red-emitting fluorescent organic@silicate core-shell nanoparticles towards bio-imaging**

### **Supplementary information**

Shridevi Shenoï-Perdoor,<sup>a</sup> Xavier Cattoën,<sup>\*a</sup> Yann Bretonnière,<sup>b</sup> Gwenaëlle Eucat,<sup>a,b</sup> Chantal Andraud,<sup>b</sup> Béatrice Gennaro,<sup>c</sup> Stéphanie Kodjikian,<sup>a</sup> Fabien Dubois<sup>a</sup> and Alain Ibanez<sup>a</sup>

<sup>a</sup>Univ. Grenoble Alpes, CNRS, Grenoble INP. Institut Néel. 38000 Grenoble, France.

<sup>b</sup>Univ Lyon, ENS de Lyon, CNRS UMR 5182, Université Lyon 1, Laboratoire de Chimie, F-69342 Lyon, France.

<sup>c</sup>Univ Grenoble Alpes, CNRS, DCM, UMR 5250, F-38000 Grenoble, France.

## 1. Synthesis of (Z)-2-(4-nitrophenyl)-3-(3,4,5-trimethoxyphenyl)acrylonitrile (II)

3,4,5-trimethoxybenzaldehyde (2.00 g, 10.19 mmol.) and 2-(4-nitrophenyl)acetonitrile (2.00 g, 12.33 mmol, 1.2 eq.) were dissolved in acetonitrile. Piperidine (30  $\mu$ L) was added and the solution heated at 40°C for 20 hours. The solution was then poured into a large volume of water (200 mL) under stirring. The precipitate thus formed was filtered, washed with water and dried. The crude was purified by chromatography on silica gel eluting with dichloromethane. Orange solid (2.46 g, yield = 71%); m.p. 161°C;  $^1\text{H-NMR}$  ( $\text{CD}_2\text{Cl}_2$ , 500 MHz,  $\delta$ /ppm) 8.30 (d,  $J = 8.9$  Hz, 2H), 7.85 (d,  $J = 8.9$  Hz, 2H), 7.64 (s, 1H), 7.26 (s, 2H), 3.92 (s, 6H), 3.88 (s, 3H);  $^{13}\text{C-NMR}$  ( $\text{CD}_2\text{Cl}_2$ , 125 MHz,  $\delta$ /ppm) 154.0, 148.3, 146.0, 141.8, 141.4, 128.8, 127.2, 124.8, 118.1, 108.8, 107.8, 61.2, 56.75; IR ( $\text{v}/\text{cm}^{-1}$ ) 2213, 1572/1505/1456, 1330, 1252; 1125, 1022. HRMS (ESI): calcd for  $\text{C}_{18}\text{H}_{16}\text{N}_2\text{NaO}_5$   $[\text{M}+\text{Na}]^+$  363.0951; found: 363.0950.

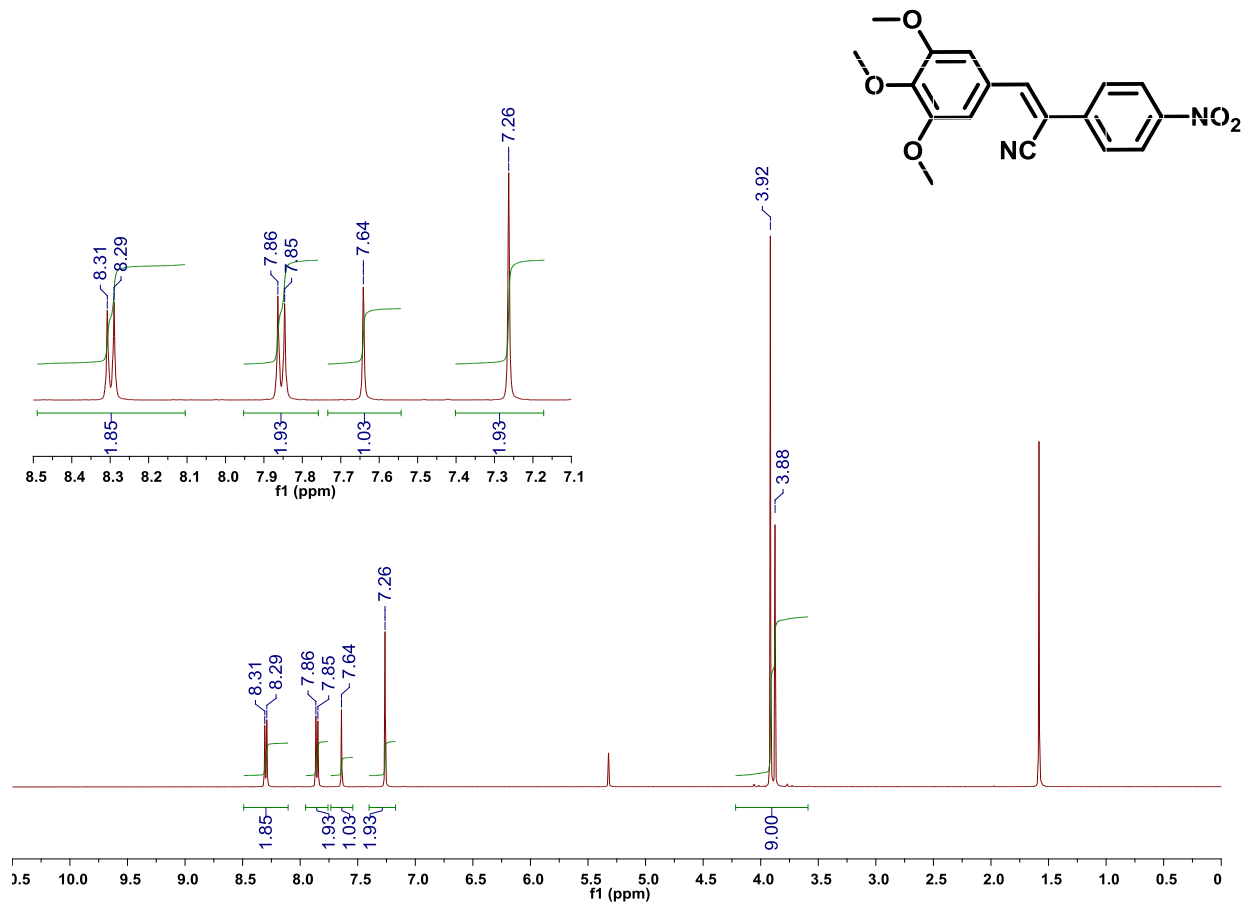


Figure S 1.  $^1\text{H-NMR}$  spectrum of compound II (500 MHz,  $\text{CD}_2\text{Cl}_2$ )

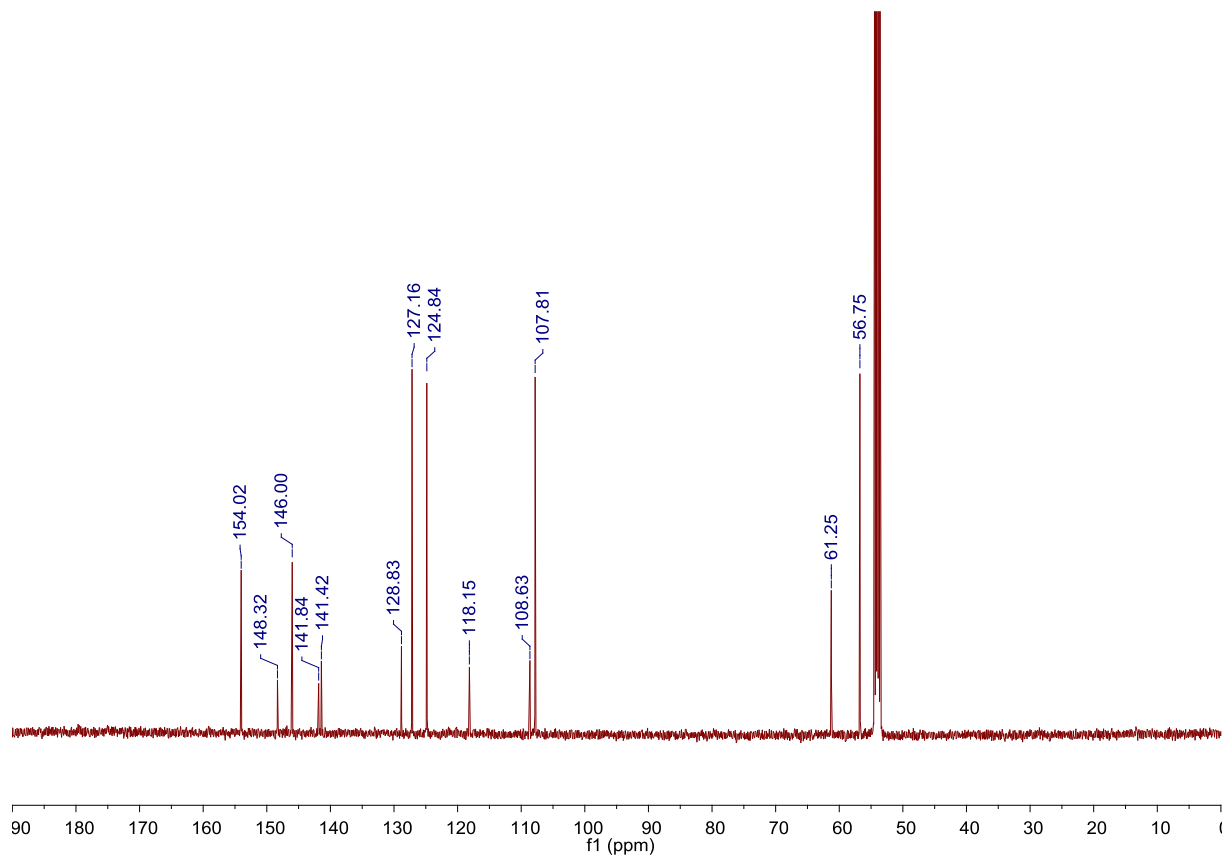


Figure S 2.  $^{13}\text{C}$  NMR spectrum of compound II (125 MHz,  $\text{CD}_2\text{Cl}_2$ )

## 2. Scheme of the spray-drying reactor

The organic@silicate core-shell NPs were synthesized in a home-made spray-dryer reactor (Figure S3). The mixture of sol and organic dye which is first introduced into a 1 L flask, is sucked into a pneumatic atomizer (TSI model 3076-Constant Output Atomizer) by a nitrogen gas flow (56 L/h), diluted with air (8 - 16 L/h) and driven into a tubular oven (35 mm diameter  $\times$  1.4 m) set to a specific temperature. The droplets generated by the atomizer initially contain a random dispersion of silicate oligomers, dye molecules and solvent, as they enter the oven. Upon their passage through the oven, solvent evaporation results in the formation of a silicate crust. Upon continued drying, dye nucleation occurs as a result of supersaturation and upon complete solvent evaporation, core-shell nanoparticles are formed at the end of the oven. The oven is connected to an electrostatic filter kept at 140 °C and charged to a potential of 10 kV where the NPs are collected on electrodes.

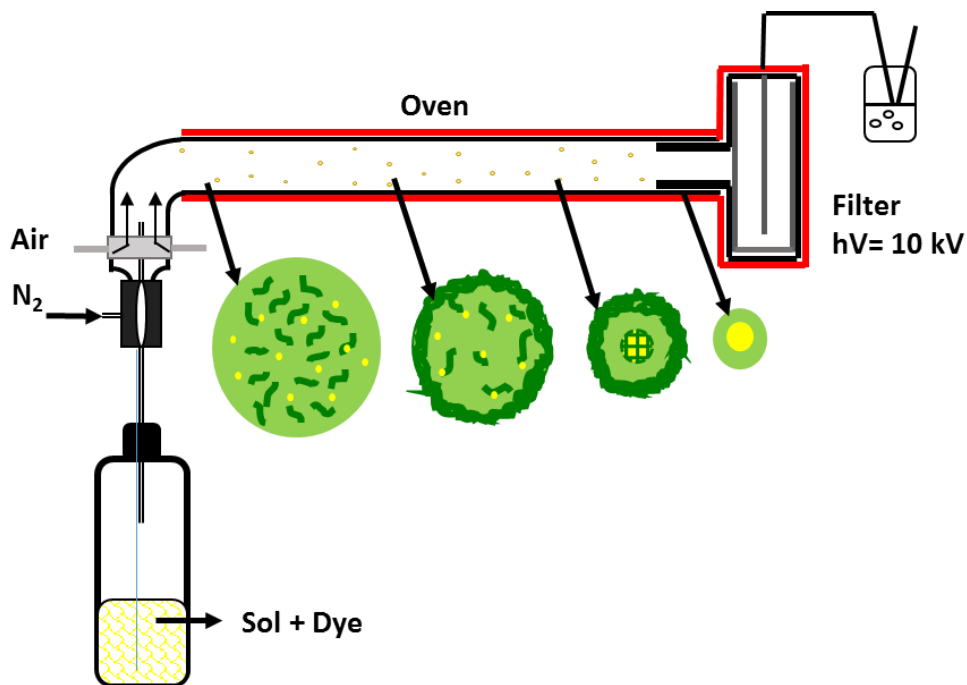


Figure S 3. Schematic illustration of the spray-drying reactor

### 3. FESEM image of dye-free nanoparticles

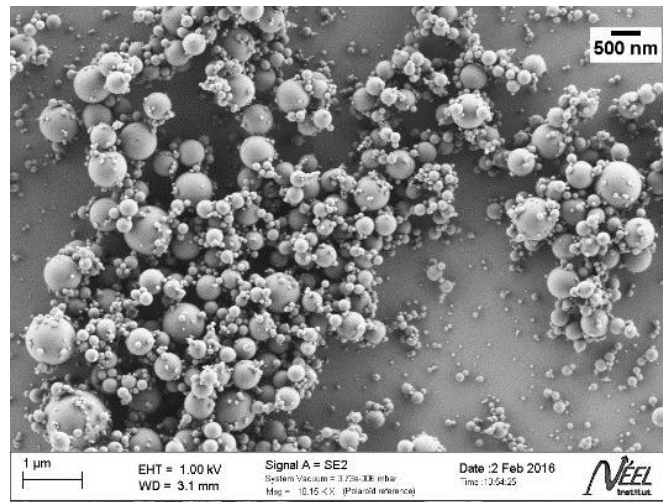


Figure S 4. FESEM image of dye-free silicate nanoparticles prepared with an oven temperature of 154 °C, s=500, h=1.

#### 4. Infrared spectra of core-shell NPs vs. Dye

The IR bands corresponding to  $\text{C}\equiv\text{N}$  ( $2210\text{ cm}^{-1}$ ) and  $\text{C}=\text{C}$  ( $1573\text{ cm}^{-1}$ ) bonds in the pure dye **I** are present in **NP-I** and absent in dye-free NPs, thereby confirming the presence of the dye **I** in the **NP-I**.

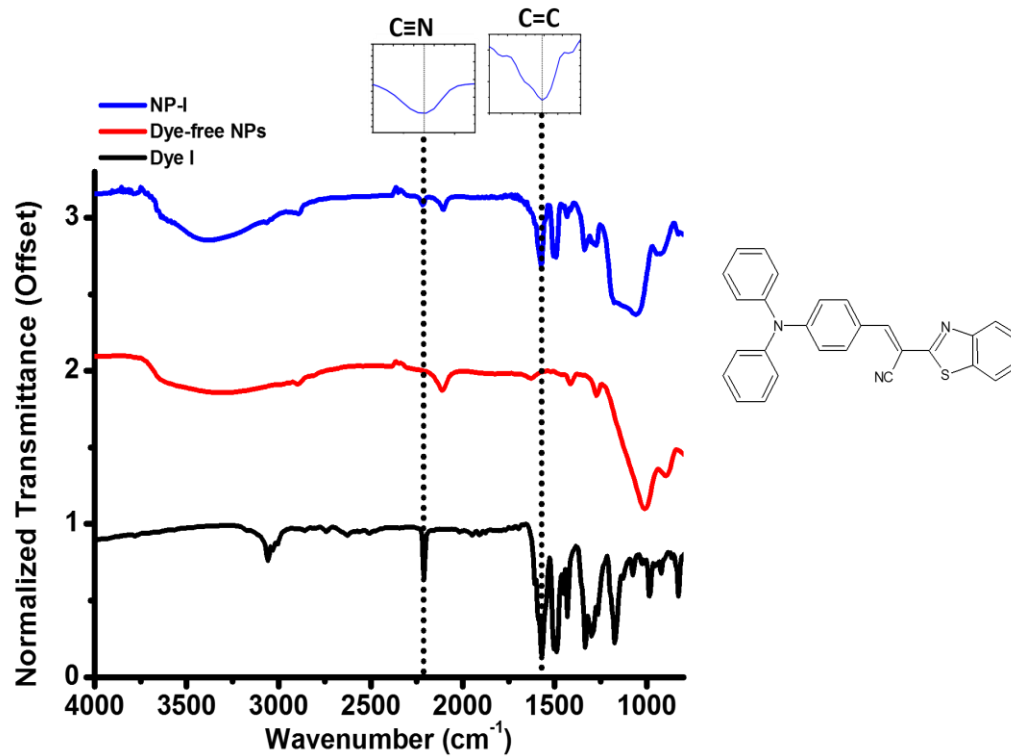


Figure S 5. Infrared spectrum of pure microcrystalline dye (**I**) vs. dye-free NPs and **NP-I**

The IR bands corresponding to C≡N ( $2213\text{ cm}^{-1}$ ) and NO<sub>2</sub> ( $1511\text{ cm}^{-1}$ ) bonds in the pure dye **II** are present in **NP-II** and absent in dye-free NPs, thereby confirming the presence of the dye **II** in the **NP-II**.

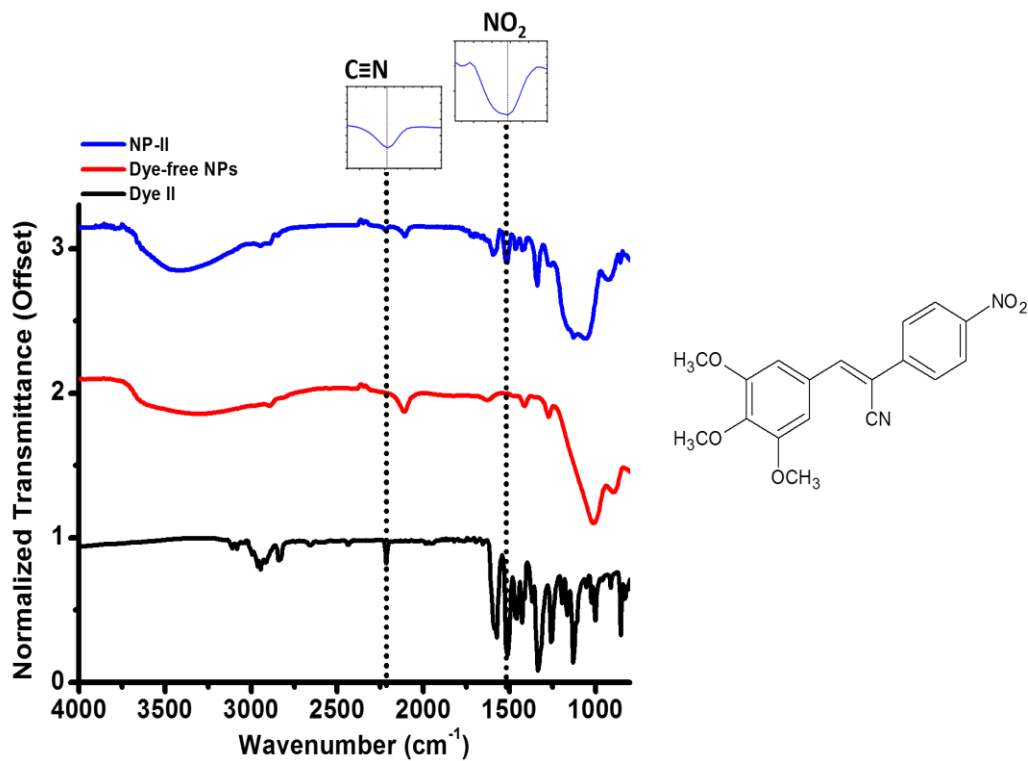


Figure S 6. Infrared spectrum of pure microcrystalline dye (**II**) vs. dye-free NPs and **NP-II**

The IR bands corresponding to  $C\equiv N$  ( $2210\text{ cm}^{-1}$ ) and  $NO_2$  ( $1515\text{ cm}^{-1}$ ) bonds in the pure dye **III** are present in **NP-III** and absent in dye-free NPs, thereby confirming the presence of the organic dye in the core-shell NPs.

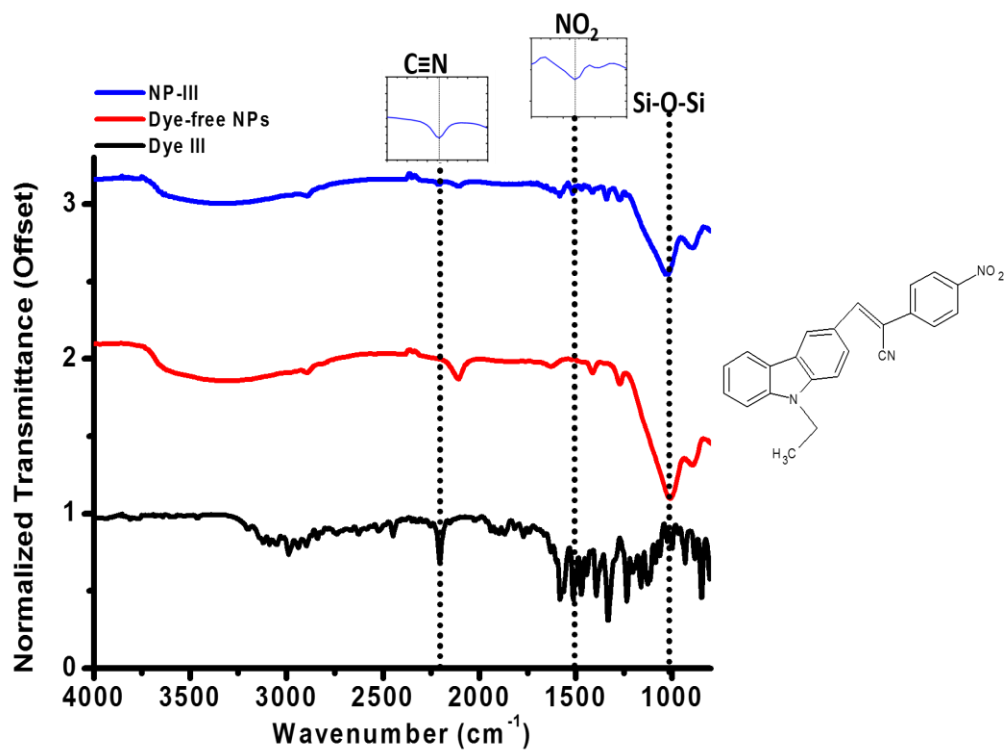


Figure S 7. Infrared spectrum of pure microcrystalline dye (**III**) vs. dye-free NPs and **NP-III**

The IR band corresponding to C=O ( $1747\text{ cm}^{-1}$ ) bond in the pure dye **IV** is present in **NP-IV** and absent in dye-free NPs, thereby confirming the presence of the dye **IV** in the **NP-IV**.

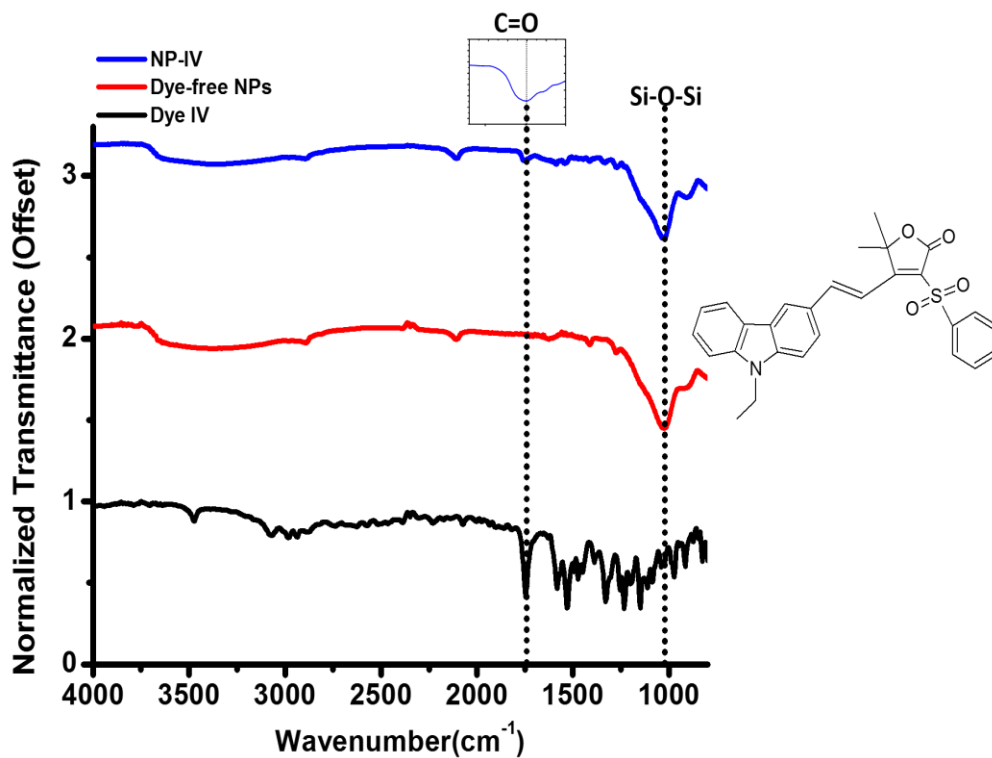


Figure S 8. Infrared spectrum of pure microcrystalline dye (**IV**) vs. dye-free NPs and **NP-IV**

## 5. Size distribution of core-shell NPs

Histograms corresponding to FESEM images of the core-shell NPs in Figure 4.

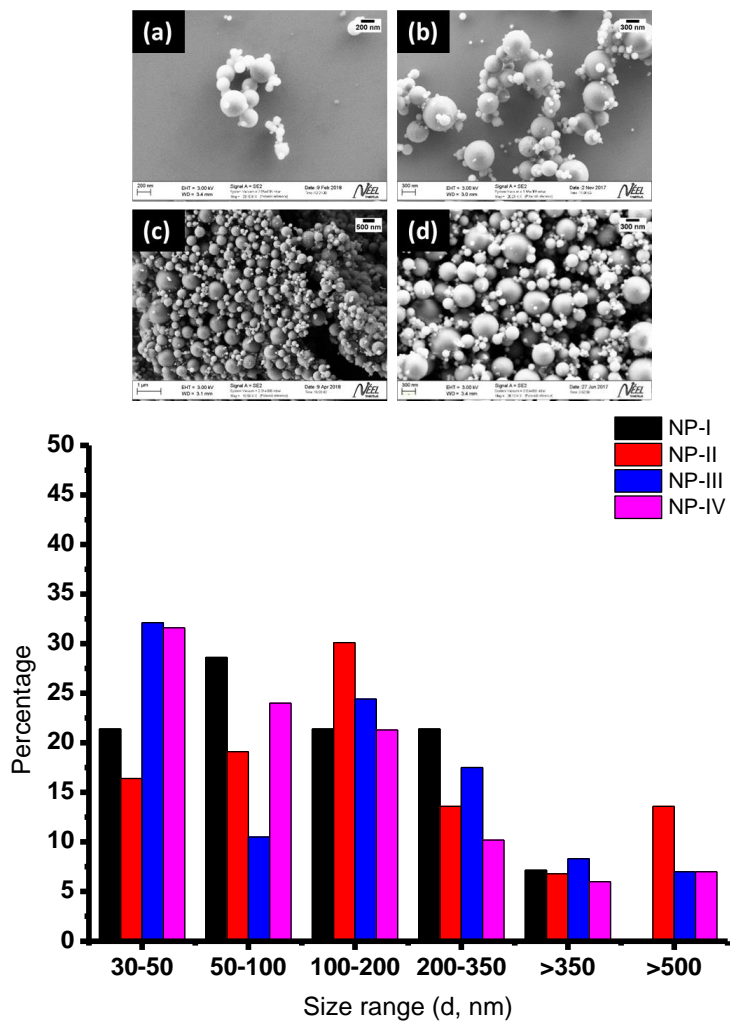


Figure S 9. Size distribution of core-shell NPs

## 6. Thermogravimetric analysis (TGA) of NP-I coupled with Differential Thermal Analysis (DTA) and Mass Spectrometry (MS) of gas exhausts

The NPs are thermally stable up to 280 °C after which the organics start to decompose. An endothermic weight loss at 340 °C, assignable to a fragmentation reaction, is followed soon after (355 °C) by a combustion leading to the production of water ( $m/z=18$ ) and carbon dioxide ( $m/z=44$ ). Thus, a highly exothermic combustion event then takes place from 450 °C associated to emission maximum of water vapor and mainly  $\text{CO}_2$  gas.

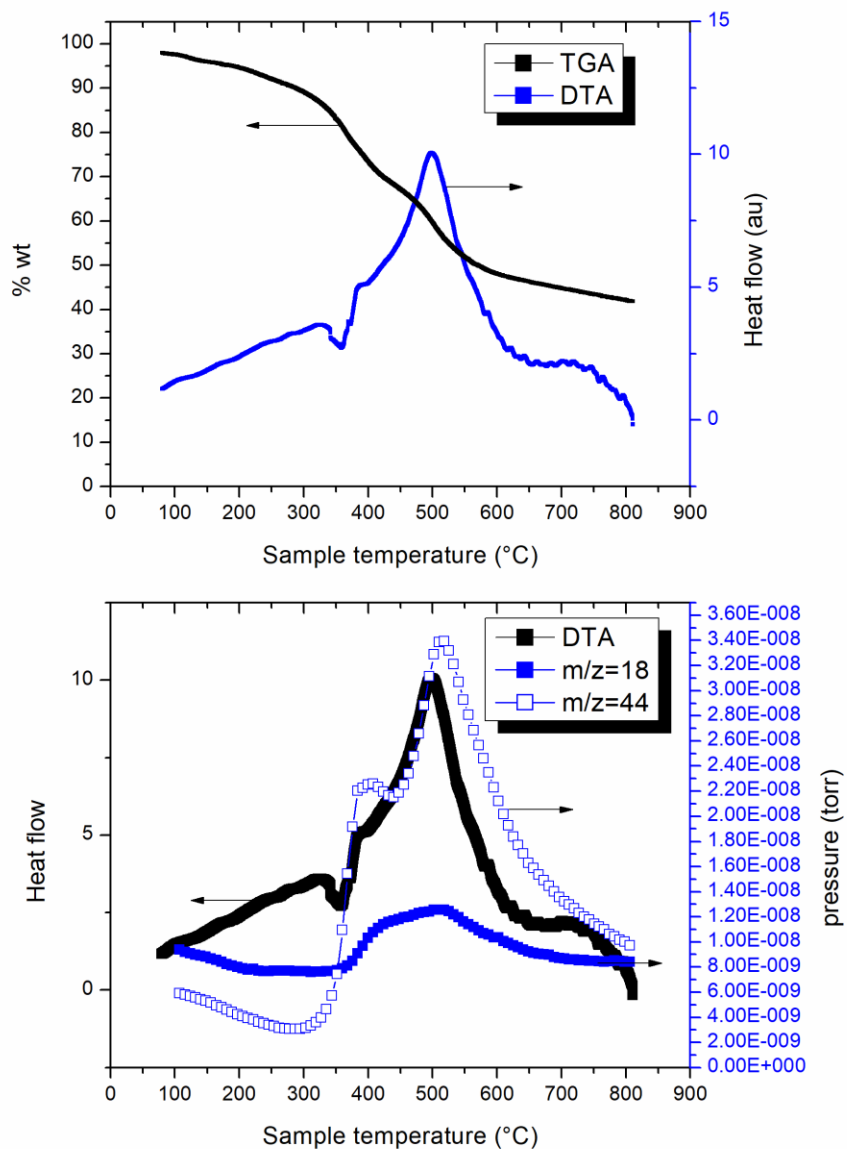


Figure S 10. TGA-DTA-MS analysis of NP-I at 8K/min under Ar/O<sub>2</sub>

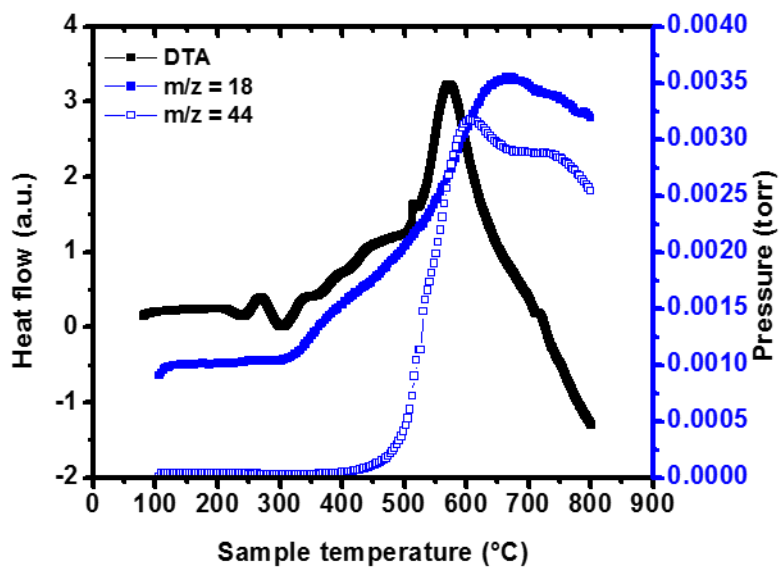
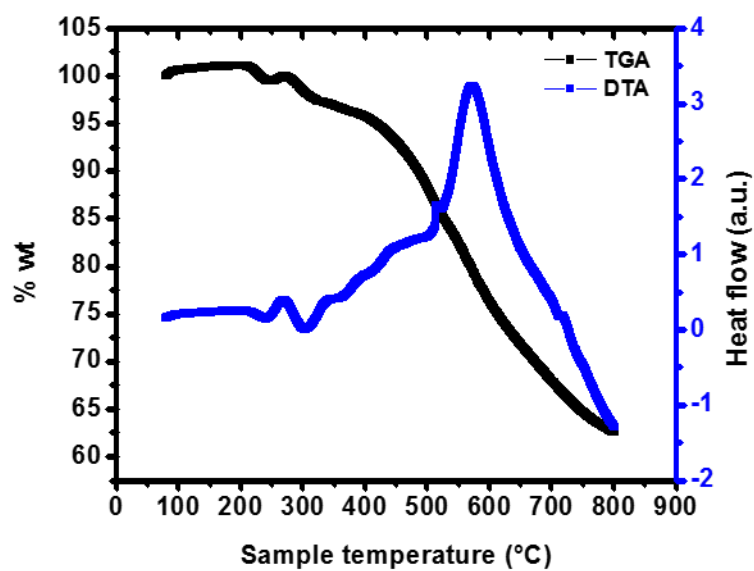


Figure S 11. TGA-DTA-MS analysis of NP-II at 8K/min under Ar/O<sub>2</sub>

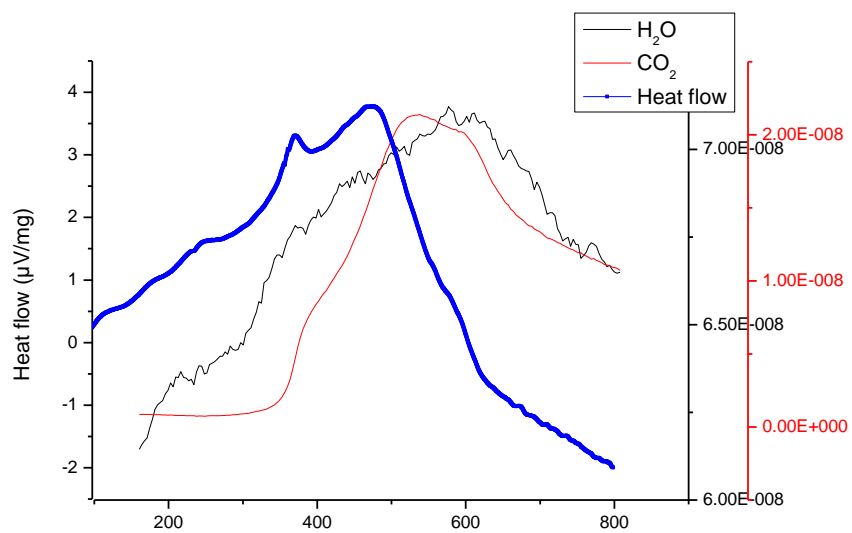
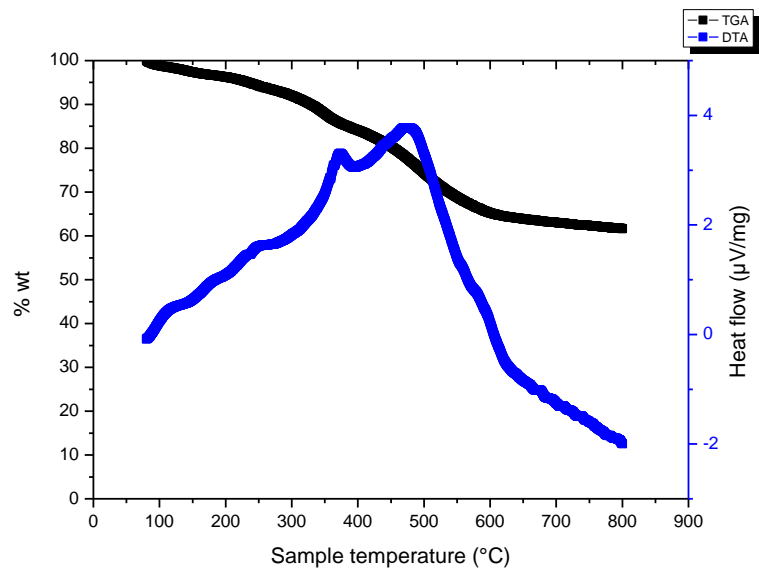


Figure S 12. TGA-DTA-MS analysis of NP-III at 8K/min under Ar/O<sub>2</sub>

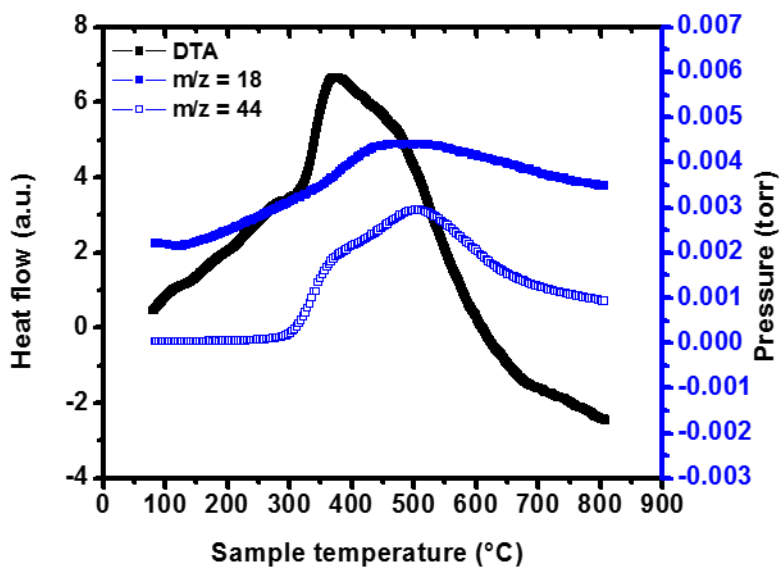
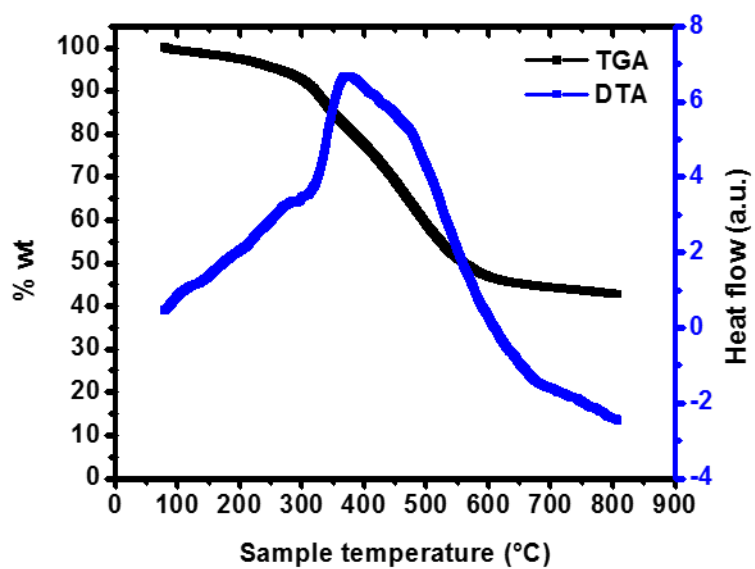


Figure S 13. TGA-DTA-MS analysis of NP-IV at 8K/min under Ar/O<sub>2</sub>

## 7. XRD

XRD data of the pure microcrystalline dyes and the core-shell NPs were collected in a Bruker D8 Advance diffractometer equipped with a monochromatic Cu K $\alpha$ 1 ( $\lambda = 1.5406 \text{ \AA}$ ) source operated in a Bragg-Brentano geometry. The data were collected from  $2\theta$ ,  $5 - 40^\circ$  with a  $0.200^\circ$  step size. A Lynxeye detector was used for data collection.

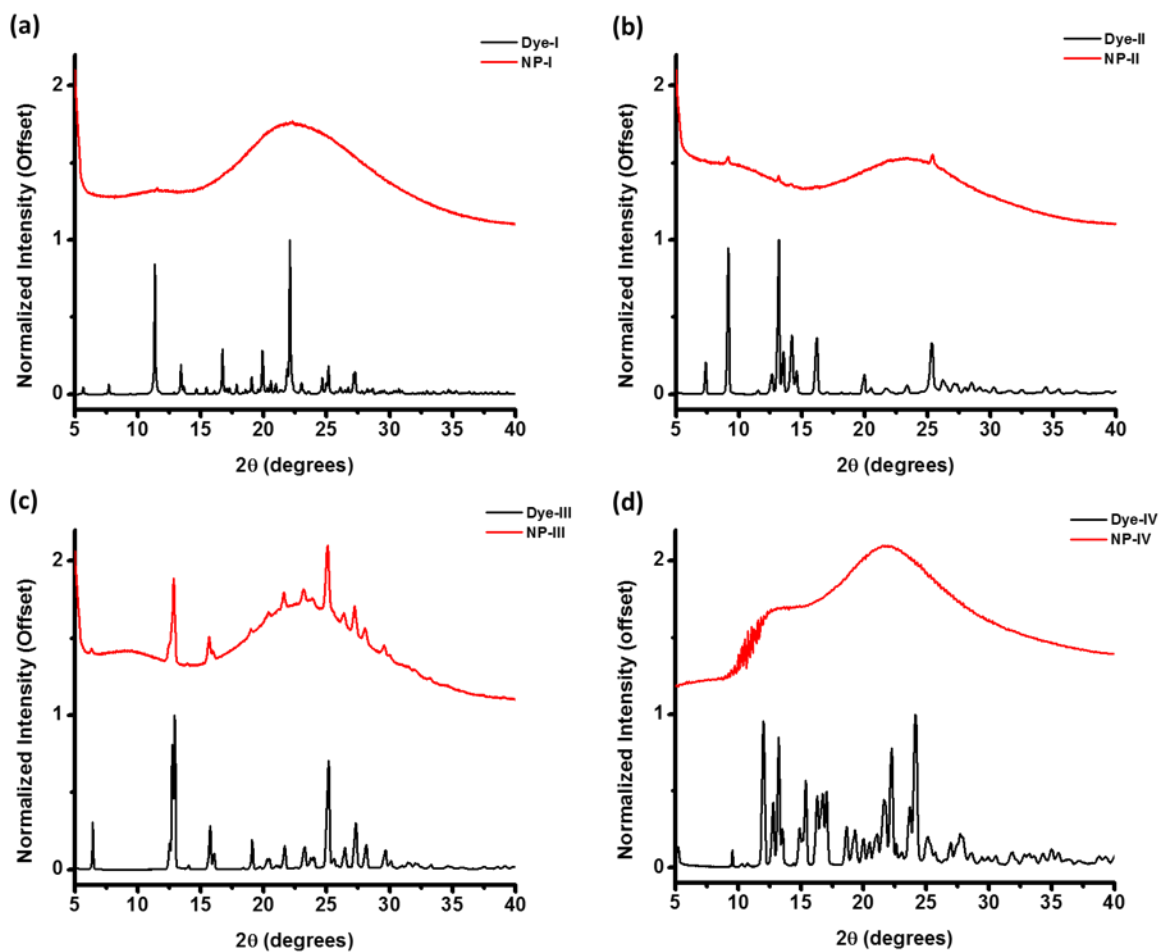


Figure S 14. XRD of (a) NP-I, (b) NP-II, (c) NP-III and (d) NP-IV (black line corresponds to pure dye and red line corresponds to core-shell NPs)

## 8. Absorbance over time

The absorbance of **NP-IV** suspension in water was monitored over 15 hours to evaluate its stability. No drop in absorbance was observed, thereby indicating stability.

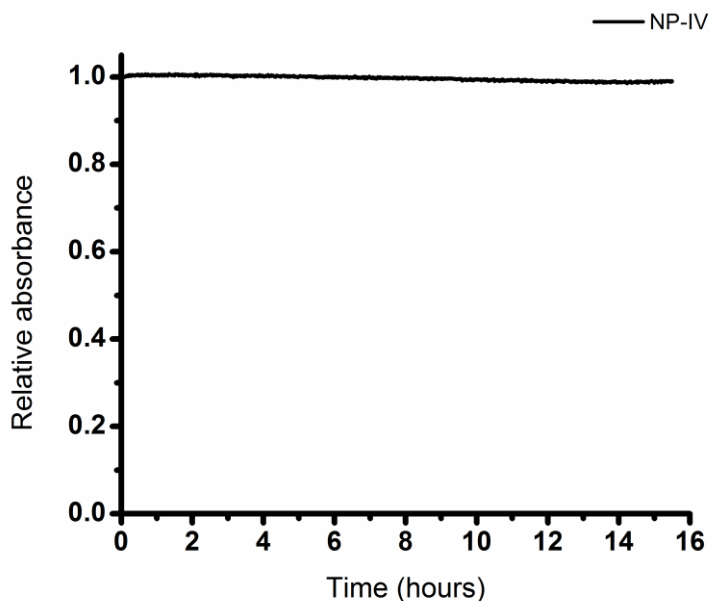


Figure S 15. Relative absorbance of NP-IV in water over 15 hours

## 7. Dynamic Light Scattering (DLS) of core-shell NPs

The size distributions of the treated NP suspensions were determined using a Malvern Zetasizer Nano ZS. Ten measurements were performed on each sample at 25 °C. General purpose analysis was used for the conversion of the autocorrelation function into size distribution.

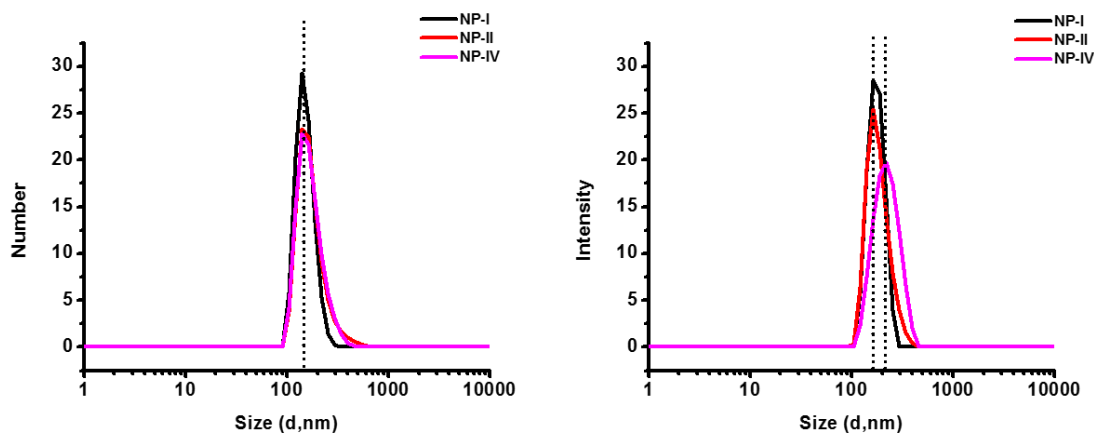


Figure S 16. DLS of core-shell NPs after treatment. The distribution in diameter is centered at ca 200 nm.

## 10. Photostability

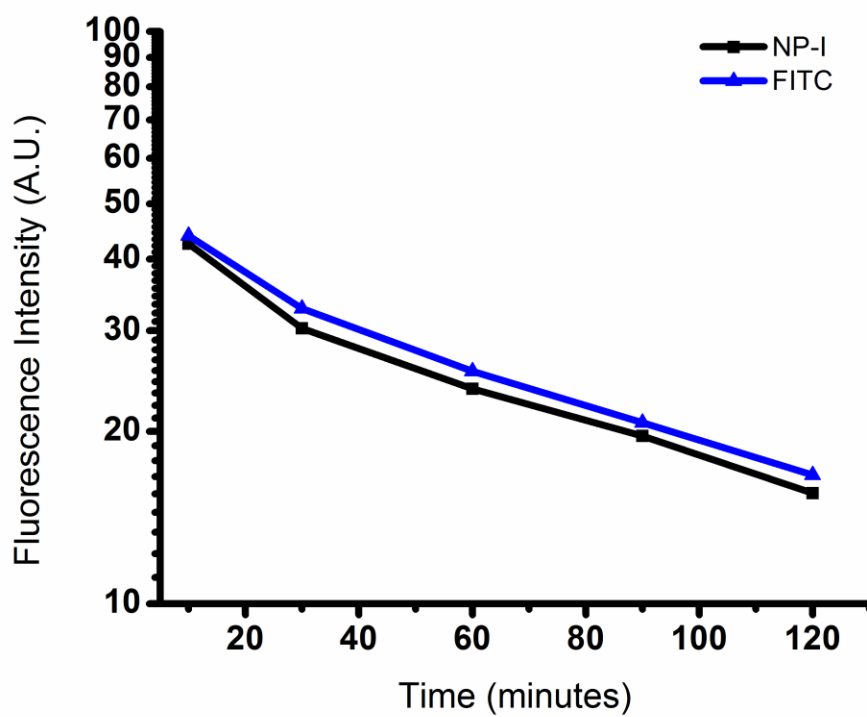


Figure S 17. Fluorescence intensity of **NP-I** and FITC (reference) recorded at different time intervals after irradiating with a 457 nm laser at 37 mW over a surface of *ca* 1 cm<sup>2</sup>